*Anal. Chem.* **1996,** *68,* 639−646

# Time- and Wavelength-Resolved Delayed-Fluorescence Emission from Acridine Yellow in an Inhomogeneous Saccharide Glass

Julius C. Fister, III, and Joel M. Harris*

*Department of Chemistry, University of Utah, Salt Lake City, Utah 84112*

**Multiwavelength time-resolved spectroscopy is employed to study the triplet-state photophysics of acridine yellow dissolved in a rigid saccharide glass. Activated reverse intersystem crossing from photoexcited triplet states to the fluorescent singlet state provides a temperature-dependent decay pathway of the triplet population. While a unimolecular relaxation of a homogeneous excited triplet population would result in single-exponential decay of the delayed-fluorescence intensity, nonexponential decay was observed at all temperatures. Multidimensional regression analysis of time- and wavelength-resolved fluorescence and phosphorescence emission is found to be a powerful method to investigate triplet-state photophysics in an inhomogeneous matrix, where two discrete populations of acridine yellow excited states are found. From the temperature dependence of their decay rates, the energy barriers to activated decay of the triplet state are determined and compared to the triplet−singlet energy gaps determined spectroscopically from the component fluorescence- and phosphorescence-band origins.**

Long-lived excited triplet states of organic dyes dispersed in rigid glasses, in polymers, or on surfaces have a number of fundamental and practical applications. For example, phosphorescence lifetimes, intensities, and anisotropy measurements have been used to investigate phase transitions in polymers such as poly(methyl methacrylate).[1] Quantitative phosphorimetry of organic molecules dissolved in saccharide glasses has been proposed as an alternative to room-temperature phosphorescence on solid surfaces such as filter paper.[2] Delayed fluorescence of adsorbed acridine has been used to characterize metal oxide surfaces.[3] Long-lived triplet states of organic dyes dissolved in lead−tin fluorophosphate glasses have recently attracted attention due to their large, easily generated nonlinear susceptibilities.[4,5] Progress in improving the performance or in understanding the fundamental behavior of these and similar systems requires developing physical models to describe the excited-state decay kinetics. However, the nonexponential decay kinetics that are often observed for molecules dissolved in rigid media[1−6] or adsorbed onto solid surfaces[3,7,8] complicate selection of appropriate physical models to describe the excited-state decay.[9,10]

Nonexponential excited-state decay data arise for a variety of reasons and can take a number of different forms. For example, solutions containing multiple fluorophores give rise to data best described by a sum of discrete single-exponential decays. On the other hand, distance-dependent quenching reactions or distributions of conformations can result in more complicated kinetics best described by one or more continuous distributions of lifetimes.[10] Unfortunately, one-dimensional kinetic measurements do not generally contain sufficient information to distinguish continuous from discrete distributions based upon statistical considerations alone unless the data are extremely precise.[9,10] Therefore, unless one can develop, a priori, a sound physical model for the form of the expected decay, or justify a particular model based on corroborating evidence, little information can be inferred from the recovered fitting parameters.[9] Interpreting decay kinetics observed in rigid or inhomogeneous media is especially challenging since site-dependent solute-solvent interactions can lead to either discrete[8] or continuous distributions of excited-state lifetimes.[11]

Acquisition of multiple emission spectra along a kinetic dimension provides significantly more resolving power than one-dimensional measurements since the evolution of component concentrations along the kinetic dimension modulates the amplitude of each component spectrum and, therefore, the shape of the observed spectra. One can test potential kinetic models against the multidimensional data in order to resolve the corresponding component spectra. Constraints placed on the form of the resolved spectra such as the shape, width of bands, and lack of negative values help guide selection of the correct kinetic model.

Early work in multidimensional emission measurements involved time- and wavelength-resolved phosphorescence[12] and fluorescence.[13] These studies addressed the analytical challenge of eliciting component spectra and lifetimes from homogenous solutions containing multiple chromophores. Wilson and Miller

(1) Ebdon, J. R.; Lucas, D. M.; Sourtar, I.; Lane, A. R.; Swanson, L. *Polymer* **1995**, *36*, 1577−1584.
(2) Chu, Y.; Hurtubise, R. J. *Anal. Lett.* **1993**, *26*, 1195−1209. Wang, J.; Hurtubise, R. J. *Appl. Spectrosc.*, in press.
(3) Oelkrug, D.; Uhl, S.; Wilkinson, F.; Willsher, C. J. *J. Phys. Chem.* **1989**, *93*, 4551−4556.
(4) Tompkin, W. R.; Boyd, R. W.; Hall, D. W.; Tick, P. A. *J. Opt. Soc. Am. B* **1987**, *4*, 1030−1034.
(5) He, K. X.; Bryant, W.; Venkateswarlu, P. *Appl. Phys. Lett.* **1991**, *59*, 1935−1937.
(6) Lewis, G. N.; Kasha, M. *J. Am. Chem. Soc.* **1944**, *66*, 2100−2116.
(7) Rosenberg, J. L.; Shombert, D. J. *J. Am. Chem. Soc.* **1960**, *82*, 3252−3257.
(8) Wang, H.; Harris, J. M. *J. Phys. Chem.* **1995**, *99*, 16999−17009.
(9) James, D. R.; Ware, W. R. *Chem. Phys. Lett.* **1985**, *120*, 455−459.
(10) Marshall, D. B. *Anal. Chem.* **1989**, *61*, 660−665.
(11) James, D. R.; Ware, W. R. *Chem. Phys. Lett.* **1985**, *120*, 450−455.
(12) Wilson, R. M.; Miller, T. L. *Anal. Chem.* **1975**, *47*, 256−266.
(13) Knorr, F. J.; Harris, J. M. *Anal. Chem.* **1981**, *53*, 272−276.

0003-2700/96/0368-0639$12.00/0 

first demonstrated kinetic and spectral resolution of multidimensional phosphorescence data by nonlinear optimization of both wavelength-dependent amplitudes (spectra) and decay rates.[12] Knorr and Harris improved the efficiency of the method by combining nonlinear optimization of only the component lifetimes with a multidimensional linear least-squares step to simultaneously resolve the component spectra.[13] While these and later[14] applications have demonstrated the enhanced precision and resolving power of a "global" multidimensional analysis, the method should be particularly informative when the shape of the resolved spectra can be related to the kinetics which drive the evolution of the component concentrations. Few studies, however, that harness the potential of this technique have appeared in the literature. Saltiel et al. employed factor analysis to resolve benzophenone phosphorescence and delayed fluorescence spectra from a data set consisting of multiple spectra acquired as a function of temperature.[15] Although factor analysis does not make use of a physical model to resolve the component spectra or underlying kinetics, a physical model was fit (in a subsequent one-dimensional analysis step) to the temperature dependence of the intensity ratio of resolved emission spectra. Best-fit parameters from the modeling step were then related to the wavelength dependence of the resolved spectra. Multidimensional least-squares analysis forms a more powerful approach by simultaneously utilizing *all* of the information in the data to guide optimization of the physical model and resolve the corresponding component spectra.

Long-lived triplet states of organic dyes solvated in a rigid glass composed of trehalose, a disaccharide, and glucose provide an interesting system on which to test these ideas. In addition to the phosphorimetry applications[2] mentioned above, the glass-forming properties of trehalose have attracted interest as a potential food preservative[16] and as a solvent which prevents protein denaturation in life forms able to endure severe desiccation.[17] We recently investigated delayed fluorescence of acridine yellow in a trehalose glass as a potential material for optical thermometry.[18] Reduced diffusion rates in the rigid glass prevent bimolecular quenching from competing with intermolecular decay processes. Therefore, the combination of an activated decay route (delayed fluorescence) and direct decay of the triplet state (phosphorescence and nonradiative decay to the ground state) determines the triplet-state lifetime at a given temperature. The large energy barrier to activated reverse-intersystem crossing and the slow phosphorescence rate result in a very high temperature sensitivity of the delayed fluorescence lifetime compared to excited state lifetimes of materials more commonly used in thermometry such as ruby or neodymium.[18] While delayed fluorescence from a homogeneous population of excited triplet states should decay as a single-exponential relaxation,[6] nonexponential decay was observed at all temperatures for this system. Since the energy barrier to activated decay of the triplet-state is reflected in both the temperature dependence of the triplet state lifetime and relative intensities and spectral origins of delayed fluorescence and phosphorescence,[19] multidimensional regression analysis of time- and wavelength-resolved emission provides a powerful method to resolve kinetic inhomogeneities in this system.

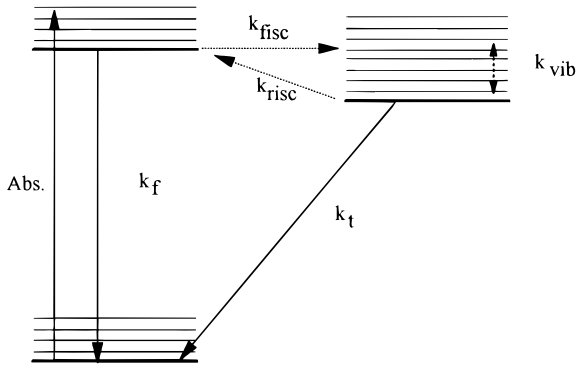


Figure 1. Energy-level diagram for the delayed fluorescence kinetics of acridine yellow.

## THEORY

**Delayed Fluorescence**. The characteristics of delayed fluorescence are described within the framework of the energy diagram shown in Figure 1. Following excitation of the ground-state dye, the majority of excited states relax within picoseconds to the lowest vibrational level of the first electronically excited singlet state $S_1$. Two pathways dominate decay of the excited singlet state. Approximately 30% decay within several nanoseconds via prompt fluorescence, $k_f$.[20] It is reasonable to assume that $S_1 \rightarrow S_0$ internal conversion to the ground state makes a small contribution to the excited singlet-state decay. This assumption is based on two factors: first, the rate of internal conversion falls off exponentially with increasing energy of the excited singlet state;[21] for singlet-state energies greater than $\sim$18 000 $cm^{-1}$,[22] internal conversion is not generally competitive with fluorescence and intersystem crossing. A second factor that would further reduce the rate of internal conversion is the requirement that the nuclei undergo a significant distortion of their equilibrium positions upon changing electronic states;[22] in a glass, changes in conformation would be inhibited by the surrounding rigid solvent matrix thus preventing a crossing to the ground-state potential surface.

Under the assumption of negligible internal conversion, the fraction of excited states that does not fluoresce undergoes forward intersystem crossing, $k_{fisc}$, to the triplet-state manifold with a quantum efficiency, $\phi_{fisc}$, that is related to the fluorescence quantum yield by $\phi_f = 1 - \phi_{fisc}$. Equilibration among the vibrational levels of the first excited triplet state occurs within picoseconds of intersystem crossing, $k_{vib}$. In fluid solutions, bimolecular quenching by oxygen and dissolved impurities establish an upper limit to triplet-state lifetimes of $\leq$1 ms. Rigid solvents dramatically reduce diffusion rates, which, as a consequence, allows the intrinsic triplet-state decay processes to proceed unperturbed by bimolecular quenching. Decay routes leading directly from the triplet state to the ground state include phosphorescence and nonradiative intersystem crossing. Acti-


(14) Beechem, J. M.; Gratton, E.; Ameloot, M.; Knutson, J. R.; Brand, L. In *Topics in Fluorescence Spectroscopy, Vol. 2: Principles*; Lakowicz, J. R., Ed.; Plenum: New York, 1991; Chapter 5.
(15) Sun, Y. P.; Sears, D. F.; Saltiel, J. *J. Am. Chem. Soc.* **1989**, *111*, 706−711.
(16) Crowe, J. H.; Crowe, L. M.; Carpenter, J. F. *Bio Pharm.* **1993**, *6(4)*, 40−43.
(17) Roser, B. *BioPharm* **1991**, *4* (8), 47−53.
(18) Fister, J. C.; Rank, D.; Harris, J. M. *Anal. Chem.* **1995**, *67*, 4269−4275.
(19) Parker, C. A.; Hatchard, C. G. *Trans. Faraday Soc.* **1961**, *57*, 1894−1904.
(20) Rank, D.; Fister, J. C.; Wacholtz, W.; Harris, J. M. Luminescence of Organic Dye Molecules in a Glass Matrix presented at the 208th National Meeting of the American Chemical Society, Washington, DC, August 1994.
(21) Siebrand, W. *J. Chem. Phys.* **1967**, *46*, 440−448.
(22) Turro, N. J. *Modern Molecular Photochemistry*; Benjamin/Cummings: Menlo Park, CA, 1978.

vated reverse intersystem crossing to the excited singlet state followed by delayed fluorescence becomes important for acridine yellow triplet states in rigid solution at temperatures above ~−70 °C.

Reverse intersystem crossing from the triplet to the excited singlet-state manifold occurs from thermally excited vibrational levels of the triplet state which have energies greater or equal to the $S_1-T_1$ energy splitting $\Delta E$.[6,19] This small fraction of the triplet population undergoes reverse intersystem crossing at a limiting rate, $k^{o}_{risc}$. Thermal equilibration between vibrational levels of the triplet state is much faster than the rate at which reverse intersystem crossing depopulates the triplet state, $k_{vib} \gg k_{risc}$. Therefore, the fraction of triplet states with sufficient energy for reverse intersystem crossing is constant and may be described by a Boltzmann distribution.[6] This leads to an expression for the effective intersystem crossing rate for the triplet population as a whole, $k_{risc}$:

$$k_{risc} = k^{\circ}_{risc} \exp(-\Delta E/kT) \tag{1}$$

where $k$ is the Boltzmann constant and $T$ is the absolute temperature. The repopulated singlet states undergo the same decay processes as those formed directly following ground-state excitation. A fraction $\phi_{fisc}$ returns to the triplet state through forward intersystem crossing. The remaining fraction, $\phi_f$, decays by fluorescence at a rate $k_f$. Reverse intersystem crossing limits the rate at which delayed fluorescence depopulates the singlet state since the lifetime of the repopulated singlet state is short compared to the time scale of reverse intersystem crossing $1/(k_f + k_{fisc}) \ll 1/k_{risc}$.

$$k_{df} = \phi_f k^{\circ}_{risc} \exp(-\Delta E/RT) \tag{2}$$

In the absence of bimolecular quenching, direct decay to the ground state, $k_t$ (given by the sum of rates of phosphorescence and nonradiative intersystem crossing), and delayed fluorescence, $k_{df}$, determine the observed triplet-state decay rate:

$$k_{obs} = k_t + \phi_f k^{\circ}_{risc} \exp(-\Delta E/kT) \tag{3}$$

Since the rates of phosphorescence and nonradiative intersystem crossing to the ground state are not generally strong functions of temperature above 77K,[22] variation in the rate of delayed fluorescence determines the temperature dependence of the triplet-state lifetime.

**Multidimensional Least-Squares Formalism**. Emission spectra acquired as a function of time after excitation may be expressed as a matrix, **D**. Within **D** the wavelength of the measurement varies as index $i$ along the rows, while time increases across the columns with index $j$. The emission intensity at any wavelength and time will be the sum of contributions from the emitting species in the sample:

$$d_{ij} = \sum_{k=1}^{n} a_{ik} c_{kj} \tag{4}$$

where $a_{ik}$ contains the wavelength variation of the phosphorescence and delayed fluorescence of the $k$th component and $c_{kj}$ is the relative contribution of the emission from the $k$th component at the $j$th time to the observed spectrum. This relationship is more conveniently expressed as a matrix product

$$\mathbf{D} = \mathbf{AC} \tag{5}$$

where **A** is a column matrix containing the combined phosphorescence and delayed fluorescence spectra of each of the two sample components and **C** is a matrix containing the time dependence of the decay of the component populations. Since the delayed fluorescence and phosphorescence of each component arise from the same population, they are not resolved in a time-dependent study. Given a model for the rows of **C** as discussed above, the least-squares estimate for the component spectra is given by

$$\hat{\mathbf{A}} = \mathbf{DC}^{T}(\mathbf{CC}^{T})^{-1} \tag{6}$$

In order to determine the lifetimes of the component spectra in **D**, the lifetimes defining the rows of **C** are optimized to minimize the squared deviations between the data and the best fit model:

$$x^2 = \sum_{i}^{n}\sum_{j}^{t}(d_{ij} - \hat{d}_{ij})^2 \tag{7}$$

where the model of the data, $\hat{d}_{ij}$ is given by $\hat{\mathbf{D}} = \hat{\mathbf{A}}\mathbf{C}$, where $\hat{\mathbf{A}}$ contains the least-squares estimated spectra.

## EXPERIMENTAL SECTION

**Formation of Disaccharide Glass**. Approximately 1 g of trehalose dihydrate crystals was ground to a powder with a mortar and pestle. An equal quantity of glucose was added to the trehalose and ground to make a 50:50 mixture. A 1.5 g sample of the sugar mixture was transferred to an ~1 cm diameter fused-silica test tube. A 1 mL aliquot of a 25 $\mu$M aqueous solution of acridine yellow was added to the sugars, stirred, and sonicated to make a solution. The tube was then suspended in a glycerol bath at 115 °C and heated until boiling ceased, ~15 min. Boiling was renewed by establishing a partial vacuum over the sugar solution. Pressure over the tube was slowly reduced over ~30 min in order to maintain slow boiling at tube temperature of 115 °C; the tube was sonicated intermittently during this process. Heating was stopped and the tube was cooled once the solution viscosity became too great to allow water vapor to escape as bubbles from the bulk solution.

**Acquisition of Time- and Wavelength-Resolved Spectra**. A xenon flash (Vivitar, Model 2800) was used for sample excitation; the fwhm of the flash was 10 $\mu$s, which is much shorter the millisecond excited-state lifetimes observed in the experiment. The flash was passed through two blue glass (Schott, BG23 3mm) filters; the resulting optical energy was ~100 mJ/cm$^{-2}$ at the sample in a 75 nm pass band centered at ~410 nm. Delayed fluorescence and phosphorescence spectra were collimated with a 50 mm fl camera lens (placed at 90° to the incident excitation) and focused onto the entrance slit of a 25 cm fl monochromator (Chromex, Model 250IS) equipped with a 600 grooves/mm grating and TE-cooled CCD (EG&G PAR). The spectral range of the detector was ~80 nm. The CCD binning scheme and shutter mode were arranged for the fastest possible data acquisi-

tion. Sets of three adjacent pixel columns along the wavelength axis were binned to minimize CCD readout time and improve the signal-to-noise ratio while spectral resolution was maintained. The mechanical shutter of the CCD was kept open during the entire experiment to minimize the delay and variation in exposure associated with rapidly opening and closing the shutter. In order to prevent the camera flash from saturating the exposed detector array, a Uniblitz shutter was placed in front of the monochromator entrance slit. The shutter opened within ~15 ms of the flash following a trigger from a photodiode. Each acquisition cycle consisted of exposure time during which charge was integrated on the detector array followed by dead time. During the dead time of 11.4 ms, the charge on the detector array was read out and swept clean prior to the next exposure. Exposure times were 10 ms at room temperature, 6.0, and 0.3 °C, 15 ms at −9 °C, and 25 ms at −78 °C.

Sample temperature was regulated by immersing the tube for several minutes in slurry baths composed of ice and salts or dry ice and organic solvents having known nominal melting temperatures.[23] Sample temperatures were monitored with a thermocouple fixed to the side of the sample cell. The sample remained immersed in the cooling baths while emission measurements were performed.

**Data Analysis**. Multidimensional nonlinear least-squares optimization of component lifetimes was performed using the SIMPLEX optimization facilities of MATLAB. The uncertainties in the component lifetimes were determined by dividing each data matrix into three smaller matrices composed of every third wavelength point in the parent matrix. Since the uncertainties at adjacent pixels are independent (the residuals of the parent data set are random with no detectable correlation) the submatrices constitute a random sample of the errors.

## RESULTS AND DISCUSSION

Time-resolved delayed fluorescence and phosphorescence spectra from acridine yellow were acquired at temperatures of −78, −9, 0.3, −21.3 °C and are shown in Figure 2. In order to capture the short wavelength edge of the delayed fluorescence spectrum, spectra were also acquired at ~6 °C with the monochromator centered at 500 nm as shown in Figure 3. For clarity, every fifth spectrum of the data set is plotted. Qualitatively, the data in Figure 2 agree with eq 3, which predicts that the contribution of thermally activated delayed fluorescence to the triplet-state decay increases with temperature, whereas the phosphorescence rate is independent of temperature. As a consequence, the intensity ratio of delayed fluorescence at 500 nm to phosphorescence at 630 nm, $I_{df}/I_p$, increases with temperature as shown in Figure 2. The multidimensional data in Figures 2 and 3 provide insight, not available in one-dimensional measurements, regarding the origin of the nonexponential delayed fluorescence kinetics of acridine yellow in the glassy saccharide matrix. For example, $I_{df}/I_p$ decreases as a function of time (see especially Figure 1c) despite the fact that $I_{df}/I_p$ should be independent of time for a single component since phosphorescence and delayed fluorescence arise from the same population of triplet states. In addition, the delayed fluorescence spectra in Figure 3 exhibit a time-dependent blue shift. These observations confirm that the data are not consistent with a single-component

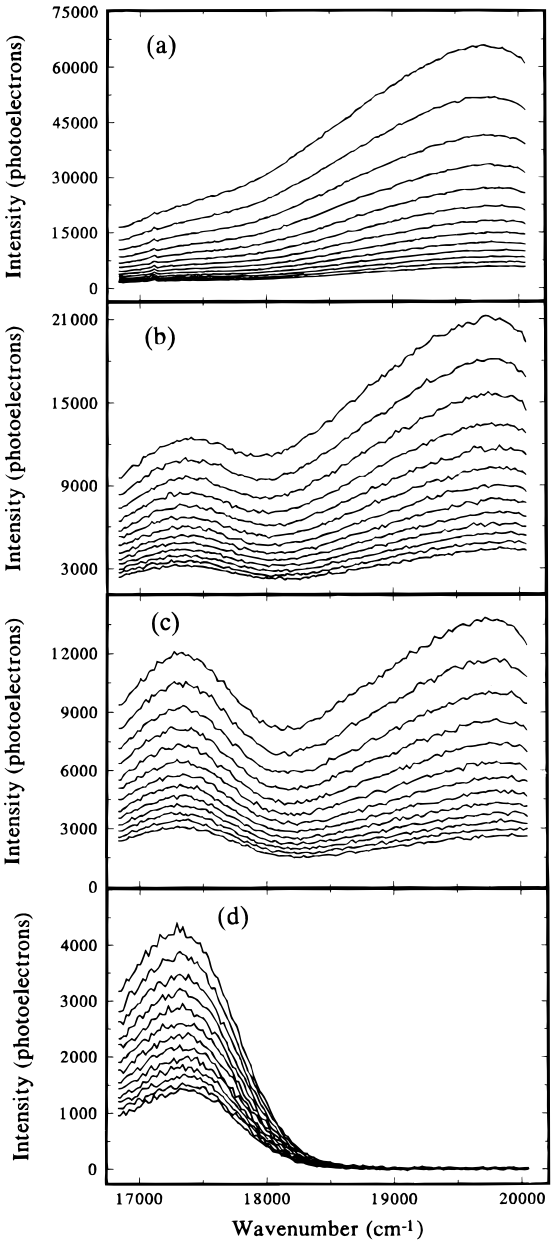


Figure 2. Time-resolved delayed fluorescence and phosphorescence spectra: (a) 21.3 °C, 107 ms time interval between plotted spectra; (b) 0.3 °C, 107 ms time interval; (c) −9.0 °C, 132 ms time interval; (d) −78.0 °C, 182 ms time interval. The actual data sets are taken at one-fifth smaller time intervals and contain 5 times more spectra than are plotted.

kinetic model. A discrete biexponential model describing two distinguishable populations of probe molecules (having slightly different barriers to activated decay) is the simplest model that is consistent with these observations.

In accord with eq 5, a design matrix, **C**, containing two rows described by first-order lifetimes $\tau_k$, was generated for each data set. The lifetimes of the two components determined by nonlinear optimization of the $\tau_k$'s are shown in Table 1. The resolved component spectra, which represent the wavelength-dependent preexponential amplitudes, are shown in Figures 4 and 5. These spectra are reasonable in their bandwidth and shape, and they have no negative-going amplitude. The simple biexponential model describes ~98% of the variance[24] in the data, and the

(23) Perrin, D. D.; Armarego, W. L. F.; Perrin, D. R. *Purification of Laboratory Chemicals*, 2nd Ed.; Pergamon Press: New York, 1980.

(24) Malinowski, E. R.; Howery, D. G. *Factor Analysis in Chemistry*; Wiley-Interscience: New York, 1980.

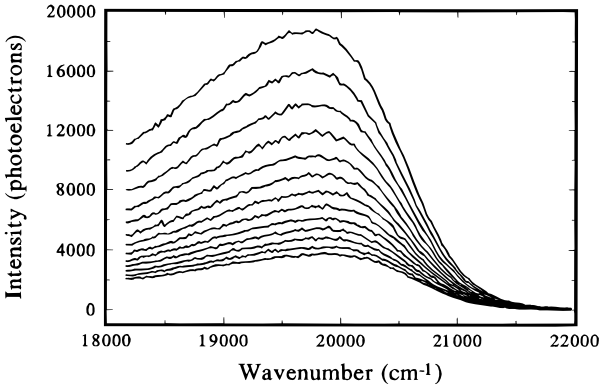


Figure 3. Time-resolved delayed fluorescence and phosphorescence spectra acquired at ~6.0 °C, 107 ms time interval. The actual data set is taken at one-fifth smaller time interval and contains 5 times more spectra than are plotted.

Table 1. Component Lifetimes (and Uncertainties) from Biexponential Fits of the Data in Figure 2

| | component lifetimes (s) | |
|---|---|---|
| temp (°C) | long-lived | short-lived |
| 21.3 | 0.49 (±0.01) | 0.208 (±0.005) |
| 0.3 | 0.94 (±0.01) | 0.352 (±0.005) |
| −9 | 1.12 (±0.02) | 0.423 (±0.007) |
| −78 | 2.0 (±0.3) | 1.0 (±0.2) |

residuals exhibit no structure along the spectral dimension. One might expect that the time-dependent blue shift of the maxima of the spectra in Figure 3 would be consistent with a single component having a fluorescence spectrum that shifts with time. Time-dependent red shifts, for example, have been observed on a subnanosecond time scale in prompt fluorescence spectra due to solvent relaxation or frequency-dependent decay rates.[25] To test whether a time-dependent shift in the fluorescence spectrum could be responsible for the data in Figure 3, a synthetic data set was constructed where the fluorescence spectrum from a single decaying component was shifted in time; a fit of these data to a biexponential model, however, produced unrealistic spectra with negative intensities.

Inhomogeneities in solvation sites or in conformations of a probe molecule can give rise to continuous distributions of excited-state lifetimes instead of discrete exponential decays.[9,10] To determine the importance of these effects on the delayed fluorescence kinetics, the data in Figures 2 were fit to a bimodal kinetic model incorporating two Gaussian lifetime distributions,[9] in which the parameters optimized were the mean component lifetimes and the widths of the distributions. The implicit assumption that the shape of the spectra within each distribution is independent of decay rate should hold for relatively narrow rate distributions. The mean lifetimes determined from the best fits to this model were indistinguishable from those listed in Table 1. The distribution widths associated with the long-lived component decay were, however, negligible (less than 10% of the mean lifetime at 21 °C and <1% at lower temperatures.). The width of the short-lived component distributions were also small, averaging 22 (±3)% of the mean lifetime. Despite the small dispersion of these component decay rates, some spectra derived from this

(25) Fee, R. S.; Milsom, J. A.; Maroncelli, M. *J. Phys. Chem.* **1991**, *95*, 5170−5181.

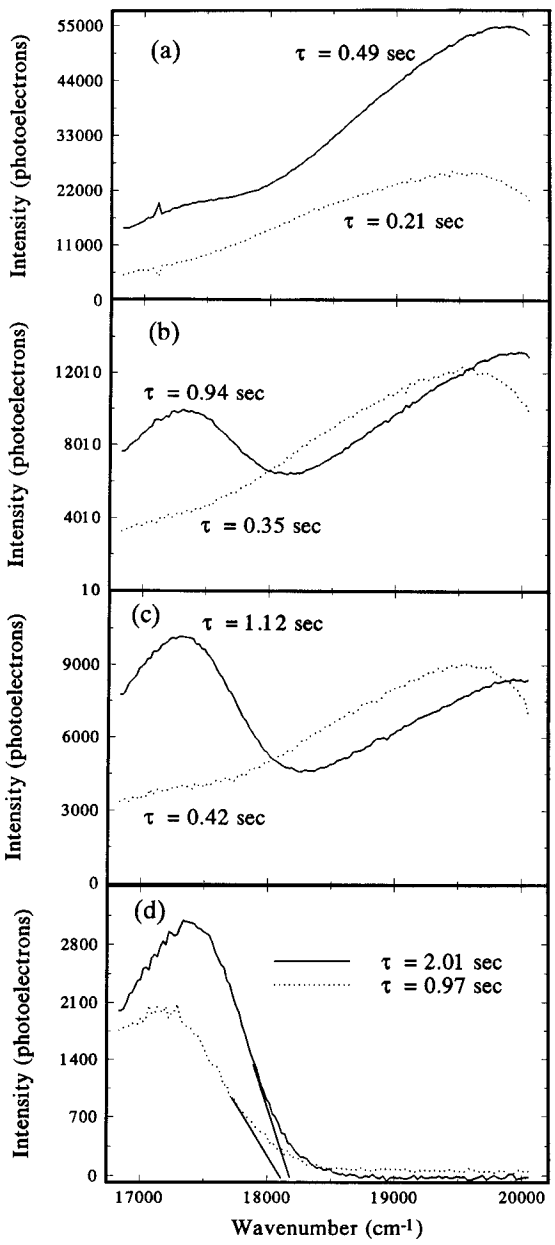


Figure 4. Resolved component emission spectra from Figure 2. Acquisition temperatures: (a) 21.3, (b) 0.3, (c) −9.0, and (d) −78.0 °C.

model exhibited negative intensity; furthermore, the activation energies determined from the intensity ratios, $I_{df}/I_p$ (see below), of the component spectra from this model did not agree with the activation energies from the component lifetimes. These results support the validity of a simple, discrete biexponential model for the decay of the acridine yellow in a saccharide glass.

Comparison of kinetic parameters derived from the temperature dependence of the component lifetimes with energetics derived from the resolved component spectra should strengthen or weaken selection of the physical model chosen to describe the system. The lifetimes of the two components decrease at approximately the same relative rate with increasing temperature, which suggests that activated decay having a similar energy barrier influences both components. To determine whether changes in the delayed-fluorescence lifetimes with temperature can be described by Arrhenius relationships, eq 3 is linearized by subtracting the direct decay rate of the triplet state, $k_t$, from

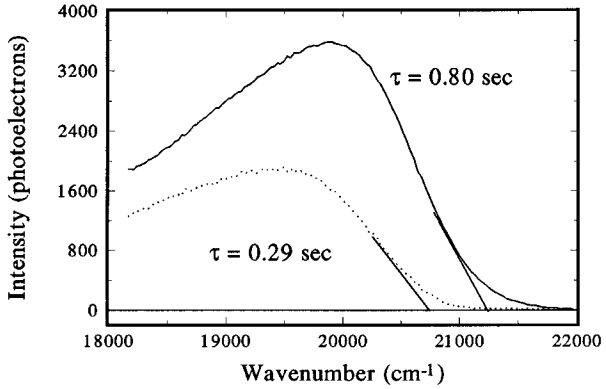


Figure 5. Resolved component emission spectra from Figure 3. Acquisition temperature, ~6.0 °C.

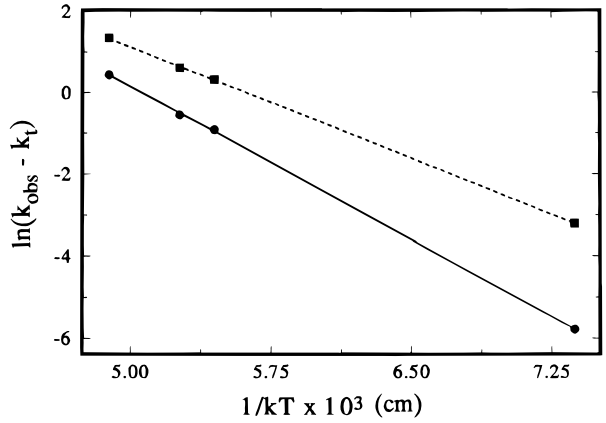


Figure 6. Arrhenius plots for acridine yellow delayed fluorescence rate as a function of temperature, for the short-lived (■) and long-lived (●) components. *x*-axis units are reciprocal wavenumbers.

both sides and taking the log

$$\ln(k_{obs} - k_t) = \ln(k_{risc}\,\phi_f) - \Delta E/kT \qquad (8)$$

Plotting the left side of eq 8 versus $1/kT$ allows the activation energy of reverse intersystem crossing, $\Delta E$, and the limiting reverse intersystem crossing rate, $k^o_{risc}$, to be determined.[6] This analysis, however, requires an estimate of the triplet decay rate in the absence of delayed fluorescence. Since thermally activated delayed fluorescence contributes to triplet decay even at −78 °C, $k_t$ was determined by a nonlinear fit of the temperature dependence of the component lifetimes to the reciprocal of eq 3, where the parameters optimized were $k_t$, $\Delta E$, and the product $\phi_f k^o_{risc}$. The triplet lifetimes thus determined were $1/k_t = 2.018$ (±0.05) s, and $1/k_t = 1.02$ (±0.03) s for the long- and short-lived components, respectively. After subtracting the inverse of these lifetimes from the observed decay rates to obtain the delayed fluorescence rate, the results were plotted according to eq 8 in Figure 6 along with the linear least-squares fit. The resulting slopes and intercepts along with their standard deviations were $\Delta E = 2540$ (±70) cm$^{-1}$ and $\ln(\phi_f k^o_{risc}) = 12.6$ (±0.1) and $\Delta E = 1845$ (±75) cm$^{-1}$ and $\ln(\phi_f k^o_{risc}) = 10.3$ (±0.3) for the long- and short-lived components, respectively. The correlation coefficient, $r^2$, was >0.999 for both plots.

The temperature dependence of the intensity ratio of delayed fluorescence to phosphorescence also follows an Arrhenius dependence.[19] The ratio $I_{df}/I_p$, is determined by the relative rates of delayed fluorescence and phosphorescence:

$$\frac{I_{df}}{I_p} = \frac{\phi_f k^\circ_{risc}}{k_p} \exp(-\Delta E/kT) \qquad (9)$$

In order to determine whether $I_{df}/I_p$ from the resolved component spectra in Figure 4 exhibits Arrhenius behavior consistent with the temperature dependence of the component lifetimes, the phosphorescence intensities must first be corrected for overlap with the delayed fluorescence spectrum. Since the delayed fluorescence spectrum of the long-lived component is similar to the prompt fluorescence spectrum measured in ethanol,[26] the contribution of the fluorescence spectrum (which maximizes at 500 nm) to the phosphorescence at 630 nm can be estimated to be ~12.5%. The corrected intensity ratios, $I_{df}/I_p$, for the long-lived component were 4.4, 1.6, 0.9, and 0.0 at temperatures 21.3, 0.3, −9.0, and −78.0 °C, respectively. The temperature dependence of the ratio is quite sensitive to the activation barrier $\Delta E$. Therefore, in order to most efficiently utilize the available degrees of freedom in the data, the corrected intensity ratios were fit to eq 9 by nonlinear optimization of $\Delta E$ and using the values of $k_t$ and $k^o_{risc}\phi_f$ determined from Arrhenius analysis of the temperature dependence of the long-lived component lifetime. The activation barrier determined from the best fit was $\Delta E = 2424$ (±20) cm$^{-1}$ which is indistinguishable at 95% confidence from the energy barrier [$\Delta E = 2540$ (±70) cm$^{-1}$)] determined from Arrhenius analysis of lifetimes in Table 1.

Determining the Arrhenius dependence of the intensity ratios of the short-lived component spectra is more difficult since the degree of overlap cannot be estimated a priori from a resolved fluorescence spectrum. Therefore, both the degree of overlap and $\Delta E$ were optimized using $k_p$ and $k^o_{risc}\phi_f$ determined from Arrhenius analysis of the short-lived component lifetimes. The degree of overlap thus determined, 18 (±0.05)%, is consistent with the shape of the resolved delayed fluorescence spectra. The activation barrier determined from the best fit was $\Delta E = 1650$ (±50) cm$^{-1}$, which is indistinguishable at 95% confidence from the activation barrier [$\Delta E = 1845$ (±75) cm$^{-1}$] determined from Arrhenius analysis of the temperature dependence of the short-lived lifetimes. Considering the uncertainty arising from spectral overlap, the agreement between $\Delta E$ determined from the temperature dependence of the lifetimes and $\Delta E$ from $I_{df}/I_p$ of the spectra is encouraging.

The Arrhenius activation energies determined above can also be compared with the enthalpy differences between excited triplet and singlet states, estimated from phosphorescence and delayed fluorescence spectra. Figure 4d shows the phosphorescence spectra resolved from the time-dependent data acquired at −78 °C. The short-wavelength origins of the delayed fluorescence spectra of the two components are shown in Figure 5. Extrapolating the high-frequency origin of each spectrum to the baseline as shown in Figures 4d and 5 allows the energy of the 0−0 transitions to be estimated. The spectroscopic enthalpy differences between singlet and triplet states thus determined were $\Delta H_s = 2975$ (±75) cm$^{-1}$ and $\Delta H_s = 2475$ (±100) cm$^{-1}$ for the long- and short-lived components, respectively. To derive an activation enthalpy from the slope of an Arrhenius plot, one must first correct

(26) Berlman, I. B. *Fluorescence Spectra of Aromatic Molecules*; Academic Press: New York, 1971.

the slope for the slight temperature dependence of the preexponential factor.[27] Correcting the Arrhenius slopes by subtracting the value of kT (=165 $cm^{-1}$) at the average temperature over which the data were acquired yields activation enthalpies of $\Delta H^{\ddagger} = 2375$ (±70) $cm^{-1}$ and $\Delta H^{\ddagger} = 1680$ (±75) $cm^{-1}$ for the long- and short-lived components respectively. These activation enthalpies are 600 (±105) and 795 (±125) $cm^{-1}$ less than the corresponding spectroscopic enthalpies.

Differences between spectroscopic and Arrhenius enthalpies can arise from conformational differences between the excited triplet state and the ground state.[7,28] When the triplet state radiates to a ground state having a different geometry, fluorescence−phosphorescence measurements can overestimate the true enthalpy difference between the first excited singlet and triplet states.[28] For example, Rosenberg and Shombert reported that the spectroscopic singlet−triplet energy difference for acriflavine (3,6-diamino-10-methylacridinium chloride) adsorbed on silica gel was ~700 $cm^{-1}$ larger than the activation enthalpy determined from the temperature dependence of delayed fluorescence.[7] The differences between the spectroscopic and activation enthalpies are indistinguishable for the short- and long-lived components. This result, along with the comparable phosphorescence origins (see Figure 4d) and different fluorescence origins (see Figure 5), suggests that differences between the triplet- and ground-state geometries of the two components are small while differences between the two excited singlet states are responsible for the different activation barriers observed for the two components.

Insight into conformational differences between the excited singlet and triplet states can also be learned by comparing the rates of forward and reverse intersystem crossing. The limiting rates of reverse intersystem crossing, $k^{o}_{risc}$, can be estimated from the intercepts of the Arrhenius plot in Figure 6, equal to the log of the product of the $k^{o}_{risc}$ and $\phi_f$. The average fluorescence quantum yield of acridine yellow in the saccharide glass has been determined to be $\phi_f = 0.33$ (±0.03).[20] Using this value of $\phi_f$, the limiting rate of reverse intersystem crossing is estimated to be $k^{o}_{risc} = 1.1 \pm 0.1 \times 10^6$ and $9.0 \pm 1.2 \times 10^4$ $s^{-1}$ for the long- and short-lived components, respectively. The forward intersystem crossing rate can be estimated from the lifetime of the first excited singlet state and the fluorescence quantum yield. Gryczynski et al. reported a fluorescence lifetime for acridine yellow of 7.7 ns in rigid poly(vinyl alcohol) film,[29] which is similar to the lifetime in ethanol, 5.1 ns.[26] The similarity of the prompt fluorescence lifetime and quantum yield ($\phi_f = 0.33$) in the rigid glass to the values in methanol ($\phi_f = 0.50$)[30] indicates that these parameters are not extremely sensitive functions of the molecular environment. Taking an average of the literature lifetime values and assuming that the contribution to the decay of the singlet states from internal conversion is negligible, the forward intersystem crossing rate is estimated to be $k_{fisc} \sim 1 \times 10^8$ $s^{-1}$. This value is ~2 and 3 orders of magnitude larger than $k^{o}_{risc}$ for the long- and short-lived components, respectively. Based on spin statistics alone, one would expect a 3-fold smaller reverse intersystem crossing rate as compared to the forward rate. The large differences between the rates of forward and reverse intersystem crossing are consistent with a significant activation entropy for reverse intersystem crossing.[28]

The activation entropy, $\Delta S^{\ddagger}$, can be determined from the limiting rate of reverse intersystem crossing (determined from the intercept of the Arrhenius plot above) using

$$\Delta S^{\ddagger} = k(\ln(k^{\circ}_{risc}) - \ln(kT/h) - 1) \qquad (10)$$

where $k$ is the Boltzmann constant.[27] The activation entropies thus determined are $\Delta S^{\ddagger} = -11.6 \pm 0.1$ and $-13.5 \pm 0.3$ $cm^{-1}$ $K^{-1}$ for the long- and short-lived components, respectively. If spin statistics alone were responsible for the entropy term, a value of $\Delta S^{\ddagger} = k \ln(1/3) = -0.75$ $cm^{-1}$ $K^{-1}$ would be expected for reverse intersystem crossing.

Two factors could be responsible for the large entropy barriers to reverse intersystem crossing. First, nonradiative transition rates between quantum states are proportional to the density of vibronic states in the final state that is isoenergetic with the initial state.[31] Since the density of states in the vibrationally excited triplet manifold is much greater than the density of states near the lowest vibrational level of the excited singlet state, the forward intersystem crossing rate should be larger than the rate of the corresponding reverse transition. The larger entropy barrier for the short-lived component may include significant conformational differences between the singlet and triplet excited states. An entropy change accompanying triplet excitation of several sensitizers has been estimated from energy transfer reactions. For example, Gessner and Scaiano found that energy transfer from triplet-state benzophenone to biphenyl was slower than that predicted from the spectroscopic enthalpy difference;[32] they attributed the slow rate to a loss of conformational freedom accompanying excitation of the biphenyl triplet state and estimated the entropy change upon triplet excitation to be $\Delta S = -2.1$ $cm^{-1}$ $K^{-1}$. The sign of the entropy change was opposite that predicted by spin statistics for this process,[32] lending even more credibility to the influence of conformational changes on triplet-state photophysics.

The agreement between the activation energies determined from Arrhenius analysis of both the temperature-dependent component lifetimes and the ratios of delayed fluorescence to phosphorescence intensities in the resolved spectra supports the choice of a simple biexponential model. The kinetic results with the resolved spectra also improve understanding of the excited -tate photophysics. The phosphorescence spectra in Figure 4d and delayed fluorescence spectra in Figure 5 indicate that the majority of the activation barrier difference between the two components results from perturbation of the excited-singlet state. This result is consistent with the presence of two different solvation environments in the rigid saccharide matrix. Solvent polarity and hydrogen-bonding effects tend to perturb the energies of ($\pi, \pi^*$) singlet states more than the corresponding triplet states since the dipole moments of excited singlet states are generally larger due to electron correlation.[33] Birks and Grzywacz observed two delayed fluorescence spectra with maxima differing by ~100 $cm^{-1}$ when proflavine dispersed in poly(methyl methacrylate) was


(27) Connors, K. A. *Chemical Kinetics: The Study of Reaction Rates in Solution;* VCH Publishers: New York, 1990.
(28) Wagner, P. J. *J. Am. Chem. Soc.* **1967**, *89*, 2820−2825.
(29) Gryczynski, I.; Kawski, A.; Nowaczyk, K.; Cherek, H. *J. Photochem.* **1985**, *31*, 265−272.
(30) Olmsted, J. O., III *J. Phys. Chem.* **1979**, *83*, 2581−2584.
(31) Avouris, P.; Gelbart, W. M.; El-Sayed, M. A. *Chem. Rev.* **1977**, *77*, 793−833.
(32) Gessner, F.; Scaiano, J. C. *J. Am. Chem. Soc.* **1989**, *107*, 7206−7207.
(33) Schulman, S. D. *Fluorescence and Phosphoresence Spectroscopy: Physiochemical Principles and Practice*; Pergamon Press: New York, 1977.

excited with 365 and 430 nm radiation.[34] They attributed this result to the presence of different ionic forms of the dye in the polymer. Due to overlap of the component absorption bands, the emission spectra were not completely resolved; the decay kinetics of the two bands were not investigated. Similarly, shifts in the prompt fluorescence spectrum of DNA−proflavine complexes of ∼800 $cm^{-1}$ have been attributed to perturbation of the excited singlet state of the dye bound in different orientations of the dye in the DNA host due to hydrogen-bonding effects and restriction of vibrational relaxation.[35]

In summary, multidimensional regression analysis of time- and wavelength-resolved fluorescence and phosphorescence emission was found to be a powerful method to investigate triplet-state photophysics of dye molecules in an inhomogeneous matrix, where two discrete populations of acridine yellow excited states are found. From the temperature dependence of the delayed-fluorescence decay rates, the energy barriers to activated decay of the triplet state were determined and compared to the triplet−singlet energy gaps determined spectroscopically from the component fluorescence- and phosphorescence-band origins. The inhomogeneous environment of the saccharide host generates two distinguishable populations of acridine yellow probe molecules in the glass, where differences in the activation barrier to delayed fluorescence for the two populations derive principally from changes in the excited singlet-state energy. The multidimensional regression method used to resolve the component responses would be applicable to other excited-state studies of site inhomogeneity in glassy solids or solid surfaces.

(34) Birks, J. B.; Grzywacz, J. *Chem. Phys. Lett.* **1967**, *1*, 187−188.
(35) Ito, H.; I'Haya, Y. I. *Int. J. Quant. Chem.* **1968**, *2* (1), 5−21.


## ACKNOWLEDGMENT

This work was supported in part by National Science Foundation under grants CHE90-10319 and CHE95-0312. Fellowship support for J.C.F. was provided by the American Chemical Society Division of Analytical Chemistry and Dupont. We appreciate the suggestion by R. J. Hurtubise to use trehalose as a host for long-lived triplet state studies.

Received for review July 24, 1995. Accepted December 1, 1995.[⊗]

AC950738C

[⊗] Abstract published in *Advance ACS Abstracts,* January 15, 1996.